Journal Pre-proof

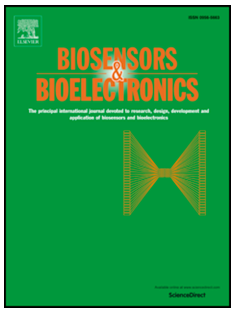

A zirconium-porphyrin MOF-based ratiometric fluorescent biosensor for rapid and ultrasensitive detection of chloramphenicol

Sha Liu, Jialei Bai, Yapeng Huo, Baoan Ning, Yuan Peng, Shuang Li, Dianpeng Han, Weijun Kang, Zhixian Gao

PII: S0956-5663(19)30880-2

DOI: https://doi.org/10.1016/j.bios.2019.111801

Reference: BIOS 111801

To appear in: *Biosensors and Bioelectronics*

Received Date: 9 August 2019

Revised Date: 25 September 2019

Accepted Date: 19 October 2019

Please cite this article as: Liu, S., Bai, J., Huo, Y., Ning, B., Peng, Y., Li, S., Han, D., Kang, W., Gao, Z., A zirconium-porphyrin MOF-based ratiometric fluorescent biosensor for rapid and ultrasensitive detection of chloramphenicol, *Biosensors and Bioelectronics* (2019), doi: https://doi.org/10.1016/j.bios.2019.111801.

A zirconium-porphyrin MOF-based ratiometric fluorescent biosensor for rapid and ultrasensitive detection of chloramphenicol

Sha Liu[a,b,+], Jialei Bai[a,+], Yapeng Huo[a,c], Baoan Ning[a], Yuan Peng[a], Shuang Li[a], Dianpeng Han[a], Weijun Kang[b,*], Zhixian Gao[a,*]

[a] Tianjin Key Laboratory of Risk Assessment and Control Technology for Environment and Food Safety, Tianjin Institute of Environment and Operational Medicine, Tianjin 300050, China

[b] School of Public Health, Hebei Medical University, Shijiazhuang 050017, China

[c] School of Public Health, Lanzhou University, Lanzhou 730000, China

[+] These authors contributed equally: Sha Liu, Jialei Bai

* Corresponding authors.
E-mail addresses: gaozhx@163.com; kangwj158@163.com

Abstract

An ultrasensitive and rapid detection of trace antibiotics is imperative for food safety and public health. Herein, we present a ratiometric fluorescent sensing strategy based on an aptamer labeled with a fluorescent dye and a highly stable zirconium-porphyrin MOF (PCN-222) as a fluorescence quencher for the high-efficiency detection of chloramphenicol (CAP). PCN-222 exhibits a strong adsorption ability toward the dye-labeled aptamer through π-π stacking, electrostatic, hydrogen bond, and coordination interactions. Experimental and simulation studies confirm that PCN-222 demonstrates a high quenching efficiency via fluorescence resonance energy transfer (FRET) and photoinduced electron transfer (PET) processes. In the presence of CAP, dye-labeled aptamers are released from the PCN-222 surface, resulting in the recovery of fluorescence. This proposed biosensor allows the complete detection of CAP within 26 min. For ratiometric measurement, its detection limit is as low as 0.08 pg

mL^{-1} with a wide detection range from 0.1 pg mL^{-1} to 10 ng mL^{-1}. It is successfully applied to analyze CAP in milk and shrimp samples, and its results are consistent with those of the commercial ELISA kit. This biosensor not only enables the rapid, ultrasensitive, and highly specific detection of CAP but also reveals excellent universality and multiplexed analysis performance.

Keywords:

Metal-organic framework; Fluorescent biosensor; Aptamer; Chloramphenicol; Ultrasensitive detection

1. Introduction

Antibiotics have been widely applied in human medicine, veterinary medicine, and food industry, due to their low cost and efficient pharmacokinetic properties (Huang et al. 2019). However, the overuse of antibiotics obtained from food can pose serious risks to human health, such as an increase in bacterial resistance and decline of immunity (Zeissig and Blumberg 2014). Therefore, the sensitive and accurate detection of antibiotics plays a vital role in food safety and public health. Various techniques, including liquid chromatography-mass spectrometer (LC-MS) (Sleegers et al. 2019), gas chromatography-mass spectrometry (GC-MS) (Tian et al. 2017), high-performance liquid chromatography (HPLC) (Xu et al. 2017), enzyme-linked immunosorbent assay (ELISA) (Wang et al. 2015), surface-enhanced Raman scattering (SERS) (Yang et al. 2016), fluorescent assay (Deng et al. 2018), and electrochemical method (Wang et al. 2019), have been employed to determine

antibiotic residues. Although these existing analytical techniques have satisfied sensitivity requirements, most of them require professional technology and expensive equipment and involve time-consuming procedures. As such, a rapid and robust method should be used to detect trace antibiotics in food samples.

Given their simplicity, high sensitivity, and multiplexed detection capacity, fluorescence-based assays have been broadly developed and proposed to detect water-soluble antibiotic contaminants (Ravikumar and Panneerselvam 2019; Miao et al. 2016; Zeng et al. 2019), such as chloramphenicol (CAP) and kanamycin (Kana), in food products. Among the developed fluorescent assays, quencher-based strategies have been widely explored because of their low background fluorescence signal and high signal-to-noise (S/N) ratio (Huang et al. 2018a). Many fluorescence quenchers, including carbon nanotubes (CNTs) (Liao et al. 2016; Ma et al. 2017), graphene oxide (GO) (Ou et al. 2019; Yugender Goud et al. 2017), g-C_3N_4 nanosheets (Duan et al. 2018a; Zheng et al. 2016) and carbon nanoparticles (Singh and Mishra 2016), MoS_2 nanostructures (Chen et al. 2017c; Huang et al. 2015), gold nanoparticles (Jiang et al. 2016; Vedova et al. 2015), quantum dots (Bhatnagar et al. 2016; Wang et al. 2018), and composite materials (Jesu Raj et al. 2015; Li et al. 2019), have been reported. These quenchers possess a good adsorption ability for dye-labeled single-stranded DNA or aptamers through π-π stacking interactions, inducing strong fluorescence quenching due to fluorescence resonance energy transfer (FRET) and/or photoinduced electron transfer (PET) process. However, the determination of antibiotic residues requires fluorescent assays with low cost, high speed, sensitivity, selectivity, and

simple implementation. None of these fluorescence quenchers can synchronously fulfill all these requirements, thereby limiting their practical and effective applications.

Metal-organic frameworks (MOFs) have been extensively investigated. MOFs are a class of porous crystalline materials synthesized by the self-assembly of inorganic-metal-containing nodes and organic linkers (Yang et al. 2017). Given their superior properties, such as large surface area, ultrahigh porosity, and tunable structures with unique physical and chemical properties (Chen et al. 2017a), they have promising applications in gas storage (Xia et al. 2015), separation (Rodenas et al. 2015), catalysis (Huang et al. 2017), sensing (Cui et al. 2015), imaging (Zhang et al. 2018), drug delivery (Duan et al. 2018b), and enzyme encapsulation (Lian et al. 2018). MOFs, such as zeolitic imidazolate framework-8 (ZIF-8) (Pan et al. 2018), UiO-66 (Wu et al. 2015), Cu(H_2dtoa) (Zhu et al. 2013), and MIL-101 (Fang et al. 2014), have also been explored as fluorescence quenchers in studies on biosensors. In comparison with typical quenchers (e.g., carbon materials), MOFs are very easily-made, cost-efficient, highly efficient, and environmentally friendly. However, these developed MOFs (e.g., UiO-66 and ZIF-8) exhibit an insufficient fluorescence quenching efficiency (QE) and a long quenching time. They also suffer from lack of water stability. These characteristics can reduce detection sensitivity, extend the analysis time, and impede their extensive uses. Therefore, a stable MOF with a superior analytical ability should be selected and fabricated to improve the sensitivity of rapid detection.

Herein, we used a highly stable zirconium-porphyrin MOF, namely, PCN-222, as a fluorescence quencher to develop a rapid and ultrasensitive fluorescence biosensor for antibiotic detection (Scheme 1). PCN-222, formulated as $Zr_6(\mu_3\text{-}OH)_8(OH)_8(H_2TCPP)_2$, was based on tetrakis(4-carboxyphenyl)porphyrin (H_2TCPP) as organic ligand and Zr_6 clusters as nodes. In comparison with other MOFs, PCN-222 could strongly and effectively adsorb dye-labeled aptamers through π-π stacking, electrostatic, hydrogen bond, and coordination interactions. As a result, a fluorescence quenching event occurred via FRET and PET processes, which were derived from the π-conjugated H_2TCPP ligands, Zr ions with a high-electron-accepting ability, and PCN-222 with a rich mesoporous structure and a high surface area. The combined effect could greatly shorten the analysis time and improve the detection sensitivity. As a proof of concept, we demonstrated here the utilization of 6-carboxyfluorescein (FAM)-labeled aptamer (FAM-aptamer) and PCN-222 to detect the target CAP. When the FAM-aptamer was adsorbed intensively onto the surface of PCN-222, the fluorescence of FAM-aptamer was quenched sharply within 1 min at high QE (>95%). In the presence of CAP, FAM-aptamers bound specifically to CAP and were released from the PCN-222 surface, inducing the fluorescence recovery of FAM-aptamers. Interestingly, the H_2TCPP ligand of PCN-222 possessed a stable emission fluorescence at 675 nm, which remained unchanged with a CAP concentration. Herein, we applied this signal as a reference to the fluorescence recovery signal from the FAM-aptamer to establish a ratiometric fluorescence biosensor. The S/N ratio increased greatly in the ratiometric

measurement, because the susceptibility against extraneous interference factors (Huang et al. 2018b), such as inhomogeneous excitation and emission, background light scattering, and photobleaching, was largely reduced. Consequently, the detection sensitivity of this strategy further enhanced. In contrast to the current novel material-based methods and commercially available ELISA kits for CAP determination, our developed PCN-222-based fluorescence assay exhibited a considerably lower detection limit of 0.08 pg mL^{-1} and a wider detection range of 0.1 pg mL^{-1} to 10 ng mL^{-1}. The overall detection time was only 26 min, which covered 1 min for quenching and 25 min for target aptamer incubation. This PCN-222-based assay displayed good long-term stability at room temperature within 1 month. It also exhibited an excellent analytical performance for CAP determination in milk and shrimp samples. This aptamer-based method displayed outstanding universality and high specificity for the multiple detection of antibiotics (e.g., CAP and Kana) by simply changing the base sequence of the aptamer. In brief, this proposed biosensor provided a strong basis for conducting fast, ultrasensitive, specific, and multiplexed detection of trace antibiotics.

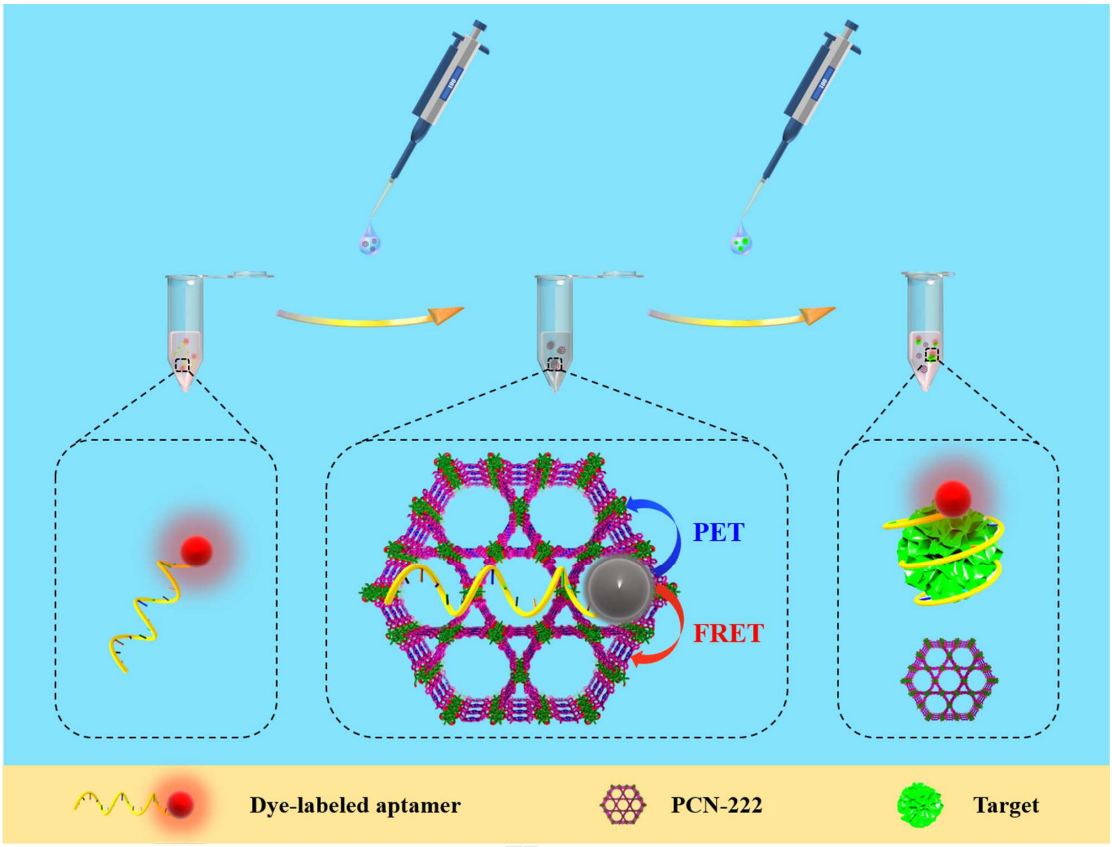

Scheme 1. Schematic illustration of the fluorescent assay with PCN-222 and dye-labeled aptamer as sensing platforms.

2. Experimental Section

The detailed procedure was provided in Supplementary Information (SI).

3. Results and Discussion

3.1 Identification of the adsorption ability of PCN-222

The PCN-222 was prepared from $ZrCl_4$ and H_2TCPP (Figures S1 and S2). PCN-222 was characterized through scanning electron microscopy (SEM), powder X-ray diffraction (PXRD), N_2 sorption isotherms, and thermogravimetric analysis (TGA) (Figures S3-S6). The adsorption ability of PCN-222 was investigated first using the FAM-aptamer of CAP as a fluorescent probe. The conjugated π-system ligands of H_2TCPP contained abundant benzene and large surface areas of PCN-222. Such

ligands allowed the strong adsorption of FAM-aptamer to the PCN-222 surface through π-π stacking interactions between the H_2TCPP ligands and the ring structures in the nucleobase (Liu et al. 2018; Zhao et al. 2015). After FAM-aptamer was adsorbed, the surface of PCN-222 appeared rough and had slightly fine cracks in the complete frame structure as seen in the SEM images (Figures 1A and 1B). Energy dispersive spectroscopy (EDS) mapping analysis demonstrated the presence of C, N, O, Zr, and P elements in PCN-222 adsorbed FAM-aptamer. The P element indicated the presence of the phosphate groups of FAM-aptamer, and its content was approximately 0.02% (w/w) in PCN-222 adsorbed FAM-aptamer. The zeta potentials (Figure S7) of PCN-222 and PCN-222 adsorbed FAM-aptamer were -17.1 and -41.9 mV, respectively, because of the negatively charged backbone of FAM-aptamer. This finding manifested that PCN-222 had a weak electrostatic interaction or a slight electrostatic repulsion with FAM-aptamer (Hao et al. 2019). The Fourier transform infrared (FTIR) spectrum (Figure S8) of PCN-222 depicted the –OH and C=O stretching vibrations of carboxyl at 3435.85 and 1713.72 cm^{-1}, respectively; by contrast, the FTIR spectrum of PCN-222 adsorbed with FAM-aptamer shifted to a lower energy at 3411.41 and 1701.63 cm^{-1}, respectively. These peak shifts were attributed to the hydrogen bond interaction between PCN-222 and FAM-aptamer bases (Zhang et al. 2014a), because the clusters of PCN-222 provided abundant hydroxyl and carbonyl groups. Moreover, the rich phosphate groups of aptamers had a strong coordination ability with inorganic Zr-O clusters (Zhang et al. 2016). The X-ray photoelectron spectroscopy (XPS) survey spectra of PCN-222 attached to

FAM-aptamer (Figures S9C and S9D) showed a new P2p peak at 133.5 eV, corresponding to the phosphate groups from FAM-aptamer. In comparison with the Zr3d spectra peaks at 182.1 and 184.6 eV for PCN-222 (Figure S9B), two other curve components at 182.7 and 185.1 eV were obtained via decomposition (Figure S9E) because of the Zr-O-P coordination (Zhu et al. 2015). Hence, the adsorption ability of PCN-222 was based on π-π stacking, weak van der Waals force, hydrogen bond, and coordination interactions, which were derived from H_2TCPP ligands, Zr ions, and the PCN-222 structure itself.

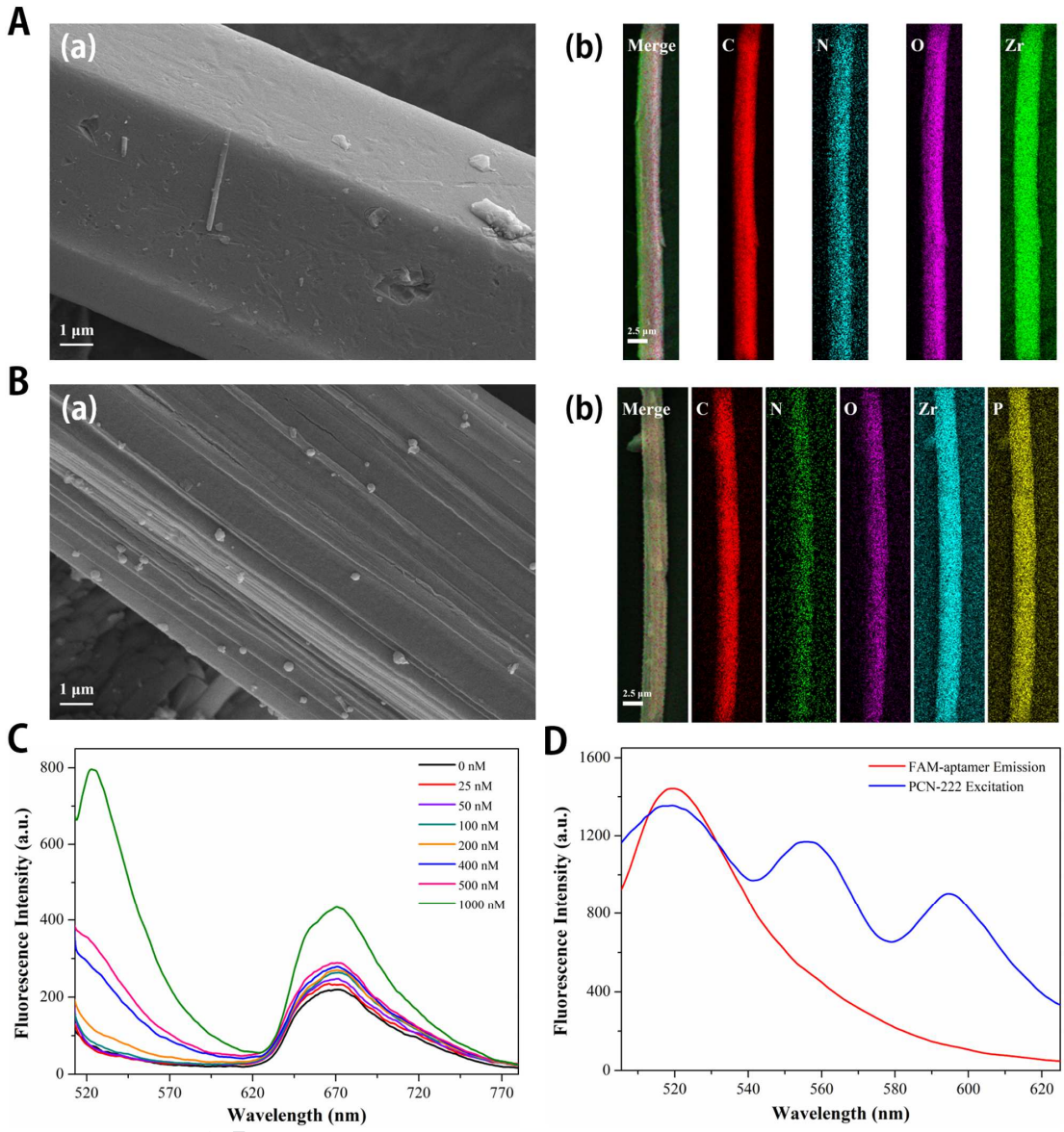

Figure 1. (A) SEM image (a) and EDS mapping analysis (b) of PCN-222. **(B)** SEM image (a) and EDS mapping analysis (b) of PCN-222 adsorbed with FAM-aptamer. **(C)** Fluorescence spectra of FAM-aptamer at different concentrations (0–1000 nM) with PCN-222 at a constant concentration of 0.2 mg mL^{-1} (excitation wavelength, 488 nm). **(D)** Fluorescence emission spectra of FAM-aptamer (excitation wavelength, 488 nm) and fluorescence excitation spectra of PCN-222 (emission wavelength, 675 nm).

3.2 Illustration of the fluorescence quenching property of PCN-222

Because of π-conjugated H_2TCPP ligands and Zr ions with a high-electron-accepting ability, the fluorescence quenching events occurred via the combined effect of FRET and PET processes. The fluorescence spectra of the FAM-aptamer solutions at

different concentrations with PCN-222 at a constant concentration were shown in Figure 1C. The fluorescence intensity of FAM-aptamer was reduced with PCN-222 (Figure S10). The astonishing results showed that the fluorescence intensity of PCN-222 at 675 nm was enhanced with the increased concentration of FAM-aptamer. The fluorescence signal of PCN-222 was roughly consistent with that of the H_2TCPP ligand (Figures S11A-S11C). Remarkably, the fluorescence excitation spectra of PCN-222 (emission wavelength of 675 nm) showed a favorable spectral overlap toward the fluorescence emission spectra at 520 nm wavelength of FAM-aptamer (Figure 1D). PCN-222 also revealed broad absorption bands in the ultraviolet-visible (UV-vis) region (Figure S11D), which had the well overlap with the emission fluorescence of FAM-aptamer. Furthermore, the time-resolved fluorescence spectra displayed that the fluorescence lifetime of FAM-aptamer decreased (He et al. 2017) after the addition of PCN-222 (Figure S12 and Table S1). Thus, the quenching event was attributed to the FRET process between the FAM dye and the H_2TCPP ligand (Liu et al. 2018) after FAM-aptamer was adsorbed onto the PCN-222 surface.

PCN-222 exhibited a broad and strong UV-vis response in the range of 300–800 nm, which inherited the Soret band ($S_0 \rightarrow S_2$ transition, ~420 nm) and four Q bands ($S_0 \rightarrow S_1$ transition, 500–700 nm) from the H_2TCPP ligand (Figure S13). With this occurrence, the electrons of PCN-222 were promoted to their excited state upon visible-light irradiation (Feng et al. 2012). After FAM-aptamer was adsorbed, the Soret band of PCN-222 exhibited a blue shift, and the Q bands decreased to three peaks with red shifts. These shifts might be attributed to the π-π interactions between the

π-conjugated H_2TCPP ligand and FAM-aptamer, as confirmed by the Raman spectrometer (Chen et al. 2014; Zhang et al. 2014b). In the Raman spectra, five vibrational bands for PCN-222 at 961.46, 1001.08, 1230.01, 1546.97, 1602.29 cm^{-1} were shifted to 963.57, 1003.89, 1234.23, 1553.11, 1606.65 cm^{-1}, respectively, for PCN-222 adsorbed with FAM-aptamer (Figure S14). Given the π-π interactions, the symmetry of H_2TCPP in the PCN-222 framework would change upon FAM-aptamer adsorption. Such change resulted in the reduction of Q-band splitting (Choi et al. 2003; Doan et al. 2005). Many studies have revealed that PCN-222 behaved like a semiconductor (Wu et al. 2015). Hence, the quenching mechanism of PET process between PCN-222 and FAM dye was speculated. The exact study was further investigated using PCN-222 and two major synthesized components, including $ZrCl_4$ and H_2TCPP. The average fluorescence QEs (%) of FAM-aptamer in the presence of PCN-222, $ZrCl_4$, and H_2TCPP reached 95.81%, 87.52%, and 75.10%, respectively (Figure S15). These findings implied that Zr^{4+} in PCN-222 also played a significant role in fluorescence quenching. Then, the structures of the geometry optimizations of the FAM molecule and the $ZrCl_4$ molecule in the ground state were calculated in accordance with density functional theory (DFT). No significant deformations were observed in molecular structures (Figure 2A). The electron-hole distributions of the molecules in the excited state were further analyzed through electron-hole theory. In Figure 2B, the green and blue atomic orbits corresponded to electrons and holes, respectively, which were involved in the orbits of excitation. In the excited state, electrons and holes were localized to $ZrCl_4$ and FAM molecules, respectively. In other

words, the electrons of FAM in the excited state were transferred to the $ZrCl_4$ molecule, generating the PET process. As illustrated in Figure 2C, the FAM dye would absorb the excitation wavelength of 488 nm to an excited state, the photogenerated electrons of which were then transferred to Zr ions with a high-electron-accepting ability of Zr-O clusters for quenching fluorescence.

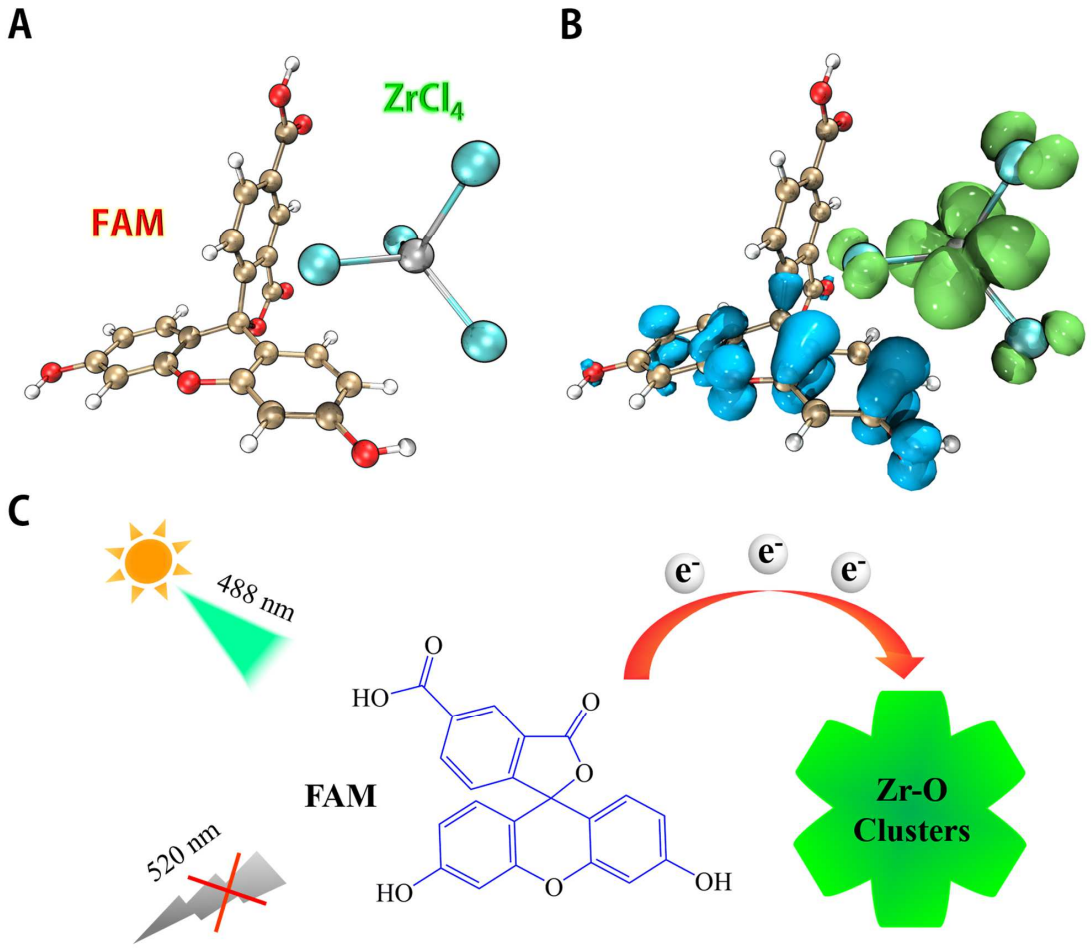

Figure 2. Calculated structures of **(A)** geometry optimizations in the ground state and **(B)** electron-hole distributions in the excited state of FAM and $ZrCl_4$ molecules. Gray, cyan, golden brown, red, and white spheres represented Zr, Cl, C, O, and H atoms, respectively. The green and blue atomic orbits represented the electrons and holes, respectively, suggesting that the electrons of FAM were transferred to the $ZrCl_4$ molecule in the excited state. **(C)** Schematic illustration of the PET process between PCN-222 and FAM for quenching fluorescence. The FAM dye could adsorb the

excitation wavelength of 488 nm to an excited state. The photogenerated electrons of FAM were then transferred to Zr ions with a high-electron-accepting ability of Zr-O clusters in PCN-222, leading to fluorescence quenching toward FAM.

3.3 Confirmation of the validity of the fluorescence assay

The binding interaction of CAP and aptamer was confirmed through microscale thermophoresis (MST). Figure S16 showed the typical curves of the normalized fluorescence time traces of MST. The binding curve of FAM-aptamer and CAP fitted at an equilibrium dissociation constant K_D equation (Wienken et al. 2010; Seidel et al. 2014) was revealed in Figure 3A. A calculated K_D value of 979.11 ± 43.16 nM (n = 3) for the FAM-aptamer-CAP binding was obtained, corresponding to K_D of 766 nM, which was first developed by a previous literature (Mehta et al. 2011). The CAP aptamer was utilized for further analysis, and the validity of the proposed biosensor platform was verified (Figure 3B). Upon the addition of PCN-222, the fluorescence of FAM-aptamer (0.5 μM) was quenched sharply at a fluorescence QE of 95.83%. It exhibited that the performance of PCN-222 for absorbing aptamer and quenching fluorescence was superior. The fluorescence intensity was recovered in the presence of CAP (1 ng mL^{-1}) at a fluorescence recovery efficiency (RE) of 13.71. The findings illustrated that FAM-aptamer was specifically bound to the target CAP (Huang et al. 2018a). The aptamer-target complex caused the rigid structure of aptamers and could effectively conceal the nucleobases and phosphate groups of aptamers, leading to the reduction of the binding affinity between PCN-222 and FAM-aptamer (Tian et al. 2015). This findings accounted for the release of FAM-aptamer from the PCN-222 surface and the fluorescence recovery. Hence, these tests demonstrated that

FAM-aptamer and PCN-222 could be utilized as favorable sensing platforms for targets.

3.4 Optimization of detection conditions

Three types of buffers were selected to achieve the maximum QE. Figure 3C showed that the average QE was 95.10% in Tris-HCl buffer (10 mM, pH 7.4) containing 150 mM NaCl, 5 mM KCl, and 5 mM $MgCl_2$. This observation was similar to the effect of 4-(2-hydroxyethyl)-1-piperazineethanesulfonic acid (HEPES) buffer (93.59%). However, the average QE in the PBS solution was lower (84.07%) because numerous HPO_4^{2-} and $H_2PO_4^-$ groups were present in the PBS solution, and they could be adsorbed or coordinated with Zr^{4+} (Wang et al. 2017). Tris-HCl buffer was chosen as the best buffer for further experiments. The concentration of PCN-222 was also optimized (Figures 3D and S17). The results exhibited that a satisfactory QE (95.66%) was obtained for the FAM-aptamer (0.5 μM) with 0.2 mg mL^{-1} of PCN-222, which was utilized for subsequent experiments. To study the quenching and recovery kinetics, we measured the time-dependent fluorescence intensity of FAM-aptamer and FAM-aptamer/PCN-222 complex in the presence of PCN-222 and CAP, respectively. FAM-aptamer could be adsorbed rapidly on the PCN-222 surface to reach equilibrium within 1 min at a high QE (>95%) (Figure 3E), which was much faster and more effective than those obtained using some of MOFs-based quenchers listed in Table S2, such as UiO-66-NH_2 (20 min with 56% QE) (Zhang et al. 2014a), and Fe_3O_4/g-C_3N_4/HKUST-1 (30 min with 87% QE) (Hu et al. 2017). The combined effect of FRET and PET accounted for the significant quenching ability of PCN-222.

Upon the addition of the target CAP, the fluorescence intensity did not further increase when the incubation time exceeded 25 min, suggesting that the reaction between PCN-222 and FAM-aptamer/CAP complex reached equilibrium (Figure 3F). Thus, 1 and 25 min were selected as the optimum absorption and incubation times for the following experiments, respectively.

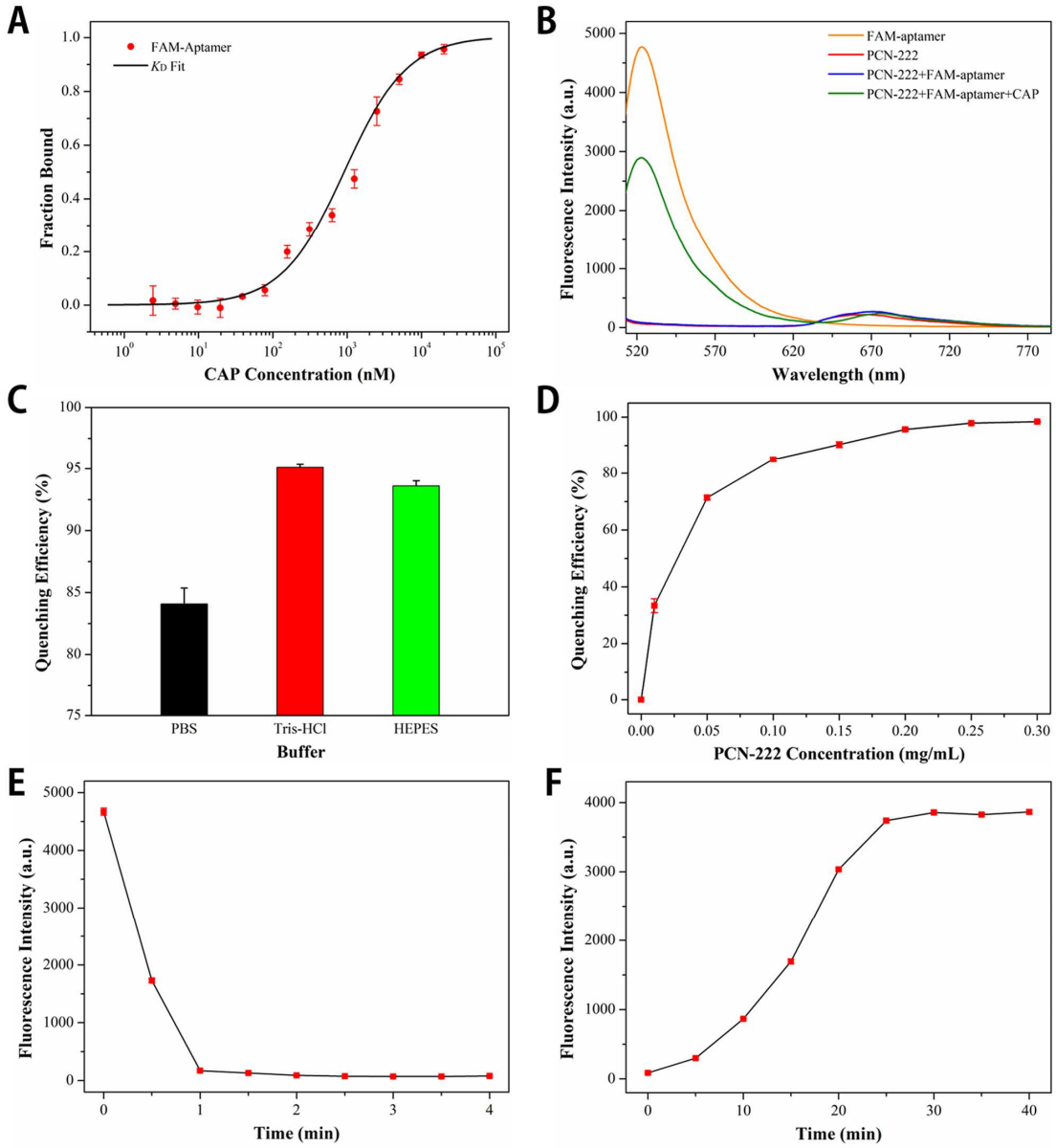

Figure 3. (A) Binding curve of FAM-aptamer (50 nM) and CAP concentrations (40 μM to 1.22 nM) measured with MST, indicating the depletion contrast upon binding. Data were mean values ± SD (standard deviation) from three parallel experiments. **(B)** Fluorescence spectra of FAM-aptamer, PCN-222, PCN-222 + FAM-aptamer, and

PCN-222 + FAM-aptamer + CAP (FAM-aptamer, 0.5 μM; PCN-222, 0.2 mg mL^{-1}; CAP, 1 ng mL^{-1}, absorption/incubation time, 30 min). **(C)** Influence of different buffers at pH 7.4 (FAM-aptamer, 0.5 μM; PCN-222, 0.2 mg mL^{-1}; adsorption/incubation time, 30 min). **(D)** Effect of PCN-222 concentration (FAM-aptamer, 0.5 μM; PCN-222, 0–0.3 mg mL^{-1}; adsorption/incubation time, 30 min). Kinetic study of the time-dependent fluorescence intensity of the **(E)** fluorescence quenching of FAM-aptamer by PCN-222 (FAM-aptamer, 0.5 μM; PCN-222, 0.2 mg mL^{-1}; adsorption time, 0–4 min) and the **(F)** fluorescence recovery of FAM-aptamer/PCN-222 complex by CAP (FAM-aptamer, 0.5 μM; PCN-222, 0.2 mg mL^{-1}; CAP, 10 ng mL^{-1}; adsorption time, 1 min; incubation time, 0–40 min). Fluorescence QEs were evaluated with fluorescence intensity at 520 nm for FAM-aptamer (excitation wavelength, 488 nm). Data were mean values ± SD from three parallel experiments.

3.5 Fluorescent detection of CAP

Under the above optimal detection conditions, the proposed assay was applied to detect CAP. As shown in Figure 4A, the fluorescence intensity at 520 nm increased gradually as the CAP concentrations increased (0.01 pg mL^{-1} to 2 mg mL^{-1}). Satisfactorily, we found that the fluorescence signal at 675 nm from the H_2TCPP ligand was not changed with different CAP concentrations. It was utilized as a reference signal for ratiometric measurement. Accordingly, the ratio of $I_{520\ nm}/I_{675\ nm}$ was used as the ratiometric fluorescence signal for subsequent analysis. The corresponding relationship between the ratio of $I_{520\ nm}/I_{675\ nm}$ and the logarithms of CAP concentrations was shown in Figure 4B. The linear detection range was from 0.1 pg mL^{-1} to 10 ng mL^{-1} (Figure 4C). R^2 was 0.9985, and the limit of detection (LOD, three times SD in the blank solution) was 0.08 pg mL^{-1}. Among the reported results of other material-based methods (Table S3), the lowest LOD was 0.52 pg mL^{-1} when the microchip electrophoresis aptasensor based on gold nanoparticle-modified stir bar was used (Zhang et al. 2019). Its detection range was from 1×10^{-3} ng mL^{-1} to 40 ng

mL^{-1}. In our work, the LOD reached a femtomole level, and the detection range was five orders of magnitude wider. The entire detection time was only 26 min, which was the most rapid among those of the listed methods. Significantly, this assay exhibited a satisfactory multiple detection performance (Figure S18), which was necessary for the rapid onsite analysis of antibiotics in food. Our method also showed the distinct fluorescence responses within 1 month (Figure S19). The results revealed that the PCN-222-based assay demonstrated exceptional long-term stability because of the strong Zr-O coordination bonds in the whole PCN-222 framework.

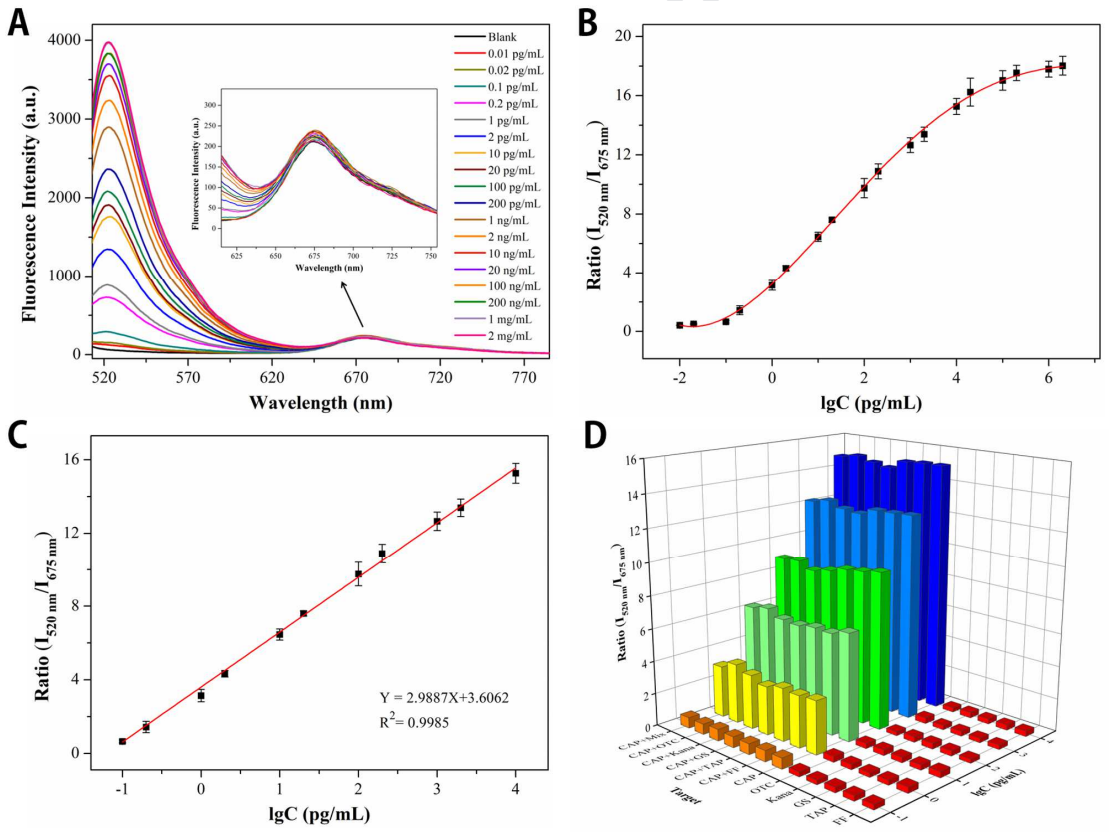

Figure 4. (A) Fluorescence spectra of FAM-aptamer and PCN-222 complexes for the detection of CAP at different concentrations (excitation wavelength, 488 nm). **(B)** Corresponding relationship and **(C)** standard curve between the ratio of $I_{520\ nm}/I_{675\ nm}$ and CAP concentrations. Data were mean values ± SD from three parallel experiments. **(D)** Specificity analysis of the proposed fluorescence assay.

3.6 Specificity of the fluorescence assay

The specificity of our method was further confirmed with other common antibiotics, including oxytetracycline (OTC), Kana, gentamicin sulfate (GS), thiamphenicol (TAP), and florfenicol (FF). Figure 4D displayed the ratio ($I_{520\ nm}/I_{675\ nm}$) responses of FAM-aptamer and PCN-222 complexes to these antibiotics at different concentrations. As expected, the ratios increased gradually as the CAP concentration increased, indicating that the more adsorbed FAM-aptamer of CAP was freed from the PCN-222 surface. Moreover, the existence of the potential interference antibiotics did not cause the fluorescence recovery of FAM-aptamer. These observations revealed that the CAP aptamer endowed this biosensor with high specificity and negligible cross-reactivity (Chen et al. 2017b; Khoshbin et al. 2018; Yan et al. 2018).

3.7 Application in real milk and shrimp samples

Spiked (0.5, 5, 50, 500, and 5000 pg mL^{-1} of CAP) milk and shrimp samples were used to determine CAP by this method and by using a commercial ELISA kit to evaluate the practical application of our proposed assay in real samples. As listed in Table 1, the average spiked recoveries displaying satisfactory results were 91.25%–105.60%. The relative standard deviation (RSD) values were 2.83%–5.02%. These data suggested the fine accuracy and good precision of the proposed assay for actual detection. For the CAP ELISA kit, the LOD was 25 pg mL^{-1} for the milk and shrimp samples (Figure S20). Hence, the average spiked recoveries and RSDs of the spiked (50, 500, and 5000 pg mL^{-1} of CAP) milk and shrimp samples were 89.91%–106.15% and 4.73%–8.51%, respectively. These results were in good agreement with our

method. In comparison with the existing commercial ELISA kits (Table S4), our assay more easily achieved fast response and had ultrasensitivity and wider detection range. These findings adequately confirmed the potential practicability of this method for CAP detection in real samples.

Table 1. Determination of CAP in milk and shrimp samples

Sample	Spiked (pg mL^{-1})	PCN-222-based assay			ELISA kit		
		Found[a] (pg mL^{-1})	Recovery (%)	RSD (%)	Found[a] (pg mL^{-1})	Recovery (pg mL^{-1})	RSD (%)
Milk	0.5	0.47984	95.97	2.83	–	–	–
	5	4.6687	93.37	3.28	–	–	–
	50	51.380	102.76	4.12	45.113	90.23	5.05
	500	493.25	98.65	3.62	466.78	93.36	4.73
	5000	5280.1	105.60	4.05	5132.3	102.65	6.78
Shrimp	0.5	0.45624	91.25	4.43	–	–	–
	5	5.1382	102.76	4.79	–	–	–
	50	48.171	96.34	4.15	47.814	95.63	8.51
	500	522.35	104.47	5.02	449.53	89.91	6.84
	5000	4721.5	94.43	3.72	5307.6	106.15	8.43

[a] n = 3, each spiked concentration was obtained from three parallel experiments.
"–" denotes "not found".

4. Conclusions

A ratiometric fluorescent sensing strategy is proposed on the basis of aptamer labeled with a fluorescent dye and a highly stable PCN-222 as a fluorescence quencher to determine CAP with high efficiency. The high speed and ultrasensitivity of this biosensor are attributed to the strong adsorption ability and the high QE of the

PCN-222 structure with H_2TCPP ligands and Zr ions. The sensitivity of PCN-222-based CAP detection in the present work is up to a femtomole level, which is considerably lower than that of existing methods. The utilization of aptamer as a recognition molecule displays outstanding universality, high specificity, and multiple analytical performance. It allows the further expansion of the extensive applications by simply changing the base sequence of the aptamer. The preparation and determination procedures are cost-efficient, easy to operate, and user friendly because of the low amount of required organic solvent and simple equipment. We anticipate the widespread application of this PCN-222-based fluorescent biosensor in food safety, medicine analysis, and environmental monitoring.

Appendix A. Supplementary data

Supplementary data related to this article can be found at

A detailed list of the figures and tables in the SI are as follows:

Figure S1. ^1H NMR spectra of TPPCOOMe
Figure S2. FTIR spectra of H_2TCPP
Figures S3-S6. SEM, PXRD, N_2 sorption isotherms, and TGA of PCN-222
Figures S7-S9. Zeta-potential analysis, FTIR spectra, and XPS spectra of PCN-222 and PCN-222 adsorbed with FAM-aptamer
Figure S10. Fluorescence intensity of FAM-aptamer at different concentrations with and without PCN-222
Figure S11. 3D fluorescent contour spectrograms and fluorescence spectra of H_2TCPP, PCN-222, and FAM-aptamer
Figure S12, Table S1. Time-resolved fluorescence spectra and fluorescence lifetimes of FAM-aptamer and FAM-aptamer mixed with PCN-222
Figure S13. UV-vis absorption spectra of H_2TCPP, PCN-222, and PCN-222 adsorbed with FAM-aptamer
Figure S14. Raman spectra of FAM-aptamer, PCN-222, and PCN-222 adsorbed with FAM-aptamer
Figure S15. Fluorescence quenching spectra of FAM-aptamer in PCN-222, $ZrCl_4$, and H_2TCPP solution

Acknowledgements

This work was supported by the National Key Research and Development Program of China (No. 2018YFC1602903, 2017YFC1601205), the National Natural Science Foundation of China (No. 81773482), and the Natural Science Foundation of Tianjin (17JCZDJC34500).

References

Bhatnagar, D., Kumar, V., Kumar, A., Kaur, I., 2016. Biosens. Bioelectron. 79, 495-499.

Chen, L., Luque, R., Li, Y., 2017a. Chem. Soc. Rev. 46(15), 4614-4630.

Chen, M., Gan, N., Zhou, Y., Li, T., Xu, Q., Cao, Y., Chen, Y., 2017b. Sens. Actuators, B 242, 1201-1209.

Chen, S.-C., Lin, C.-Y., Cheng, T.-L., Tseng, W.-L., 2017c. Adv. Funct. Mater. 27(41).

Chen, Y., Han, S., Li, X., Zhang, Z., Ma, S., 2014. Inorg. Chem. 53(19), 10006-10008.

Choi, M.Y., Pollard, J.A., Webb, M.A., McHale, J.L., 2003. J. Am. Chem. Soc. 125(3), 810-820.

Cui, Y., Song, R., Yu, J., Liu, M., Wang, Z., Wu, C., Yang, Y., Wang, Z., Chen, B., Qian, G., 2015. Adv. Mater. 27(8), 1420-1425.

Deng, J., Liu, Y., Lin, X., Lyu, Y., Qian, P., Wang, S., 2018. Sens. Actuators, B 273, 1495-1500.

Doan, S.C., Shanmugham, S., Aston, D.E., McHale, J.L., 2005. J. Am. Chem. Soc. 127(16), 5885-5892.

Duan, J., Zhang, Y., Yin, Y., Li, H., Wang, J., Zhu, L., 2018a. Sens. Actuators, B 257, 504-510.

Duan, Y., Ye, F., Huang, Y., Qin, Y., He, C., Zhao, S., 2018b. Chem. Commun. 54(42), 5377-5380.

Fang, J.M., Leng, F., Zhao, X.J., Hu, X.L., Li, Y.F., 2014. Analyst 139(4), 801-806.

Feng, D., Gu, Z.Y., Li, J.R., Jiang, H.L., Wei, Z., Zhou, H.C., 2012. Angew. Chem., Int. Ed. 51(41), 10307-10310.

Hao, Y.B., Shao, Z.S., Cheng, C., Xie, X.Y., Zhang, J., Song, W.J., Wang, H.S., 2019. ACS Appl. Mater. Interfaces 11(35), 31755-31762.

He, J., Li, G., Hu, Y., 2017. Microchim. Acta 184(7), 2365-2373.

Hu, S., Ouyang, W., Guo, L., Lin, Z., Jiang, X., Qiu, B., Chen, G., 2017. Biosens. Bioelectron. 92, 718-723.

Huang, X., He, Z., Guo, D., Liu, Y., Song, J., Yung, B.C., Lin, L., Yu, G., Zhu, J.J., Xiong, Y., Chen, X., 2018a. Theranostics 8(13), 3461-3473.

Huang, X., Song, J., Yung, B.C., Huang, X., Xiong, Y., Chen, X., 2018b. Chem. Soc. Rev. 47(8), 2873-2920.

Huang, Y., Shi, Y., Yang, H.Y., Ai, Y., 2015. Nanoscale 7(6), 2245-2249.

Huang, Y., Zheng, J., Wang, L., Duan, X., Wang, Y., Xiang, Y., Li, G., 2019. Biosens. Bioelectron. 127, 45-49.

Huang, Y.B., Liang, J., Wang, X.S., Cao, R., 2017. Chem. Soc. Rev. 46(1), 126-157.

Jesu Raj, J.G., Quintanilla, M., Mahmoud, K.A., Ng, A., Vetrone, F., Zourob, M., 2015. ACS Appl. Mater. Interfaces 7(33), 18257-18265.

Jiang, X., Feng, D.-Q., Liu, G., Fan, D., Wang, W., 2016. Sens. Actuators, B 232, 276-282.

Khoshbin, Z., Verdian, A., Housaindokht, M.R., Izadyar, M., Rouhbakhsh, Z., 2018. Biosens. Bioelectron. 122, 263-283.

Li, X., Wu, D., Ma, H., Wang, H., Wang, Y., Fan, D., Du, B., Wei, Q., Zhang, N., 2019. Biosens. Bioelectron. 131, 136-142.

Lian, X., Huang, Y., Zhu, Y., Fang, Y., Zhao, R., Joseph, E., Li, J., Pellois, J.P., Zhou, H.C., 2018. Angew. Chem., Int. Ed. 57(20), 5725-5730.

Liao, Q.G., Wei, B.H., Luo, L.G., 2016. Microchim. Acta 184(2), 627-632.

Liu, Y., Hou, W., Xia, L., Cui, C., Wan, S., Jiang, Y., Yang, Y., Wu, Q., Qiu, L., Tan, W., 2018. Chem. Sci. 9(38), 7505-7509.

Ma, K., Wang, H., Li, H., Xu, B., Tian, W., 2017. Sens. Actuators, B 253, 92-96.

Mehta, J., Van Dorst, B., Rouah-Martin, E., Herrebout, W., Scippo, M.L., Blust, R., Robbens, J., 2011. J. Biotechnol. 155(4), 361-369.

Miao, Y.B., Ren, H.X., Gan, N., Cao, Y., Li, T., Chen, Y., 2016. Biosens. Bioelectron. 81, 454-459.

Ou, X., Zhan, S., Sun, C., Cheng, Y., Wang, X., Liu, B., Zhai, T., Lou, X., Xia, F., 2019. Biosens. Bioelectron. 124-125, 199-204.

Pan, Y., Zhan, S., Xia, F., 2018. Anal. Biochem. 546, 5-9.

Ravikumar, A., Panneerselvam, P., 2019. Analyst 144(7), 2337-2344.

Rodenas, T., Luz, I., Prieto, G., Seoane, B., Miro, H., Corma, A., Kapteijn, F., Llabres, I.X.F.X., Gascon, J., 2015. Nat. Mater. 14(1), 48-55.

Seidel, S.A.I., Markwardt, N.A., Lanzmich, S.A., Braun, D., 2014. Angew. Chem. Int. Ed. 53(30), 7948-7951.

Singh, V., Mishra, A.K., 2016. Sens. Actuators, B 227, 467-474.

Sleegers, N., van Nuijs, A.L.N., van den Berg, M., De Wael, K., 2019. Anal. Chem. 91(3), 2035-2041.

Tian, J., Liu, Q., Shi, J., Hu, J., Asiri, A.M., Sun, X., He, Y., 2015. Biosens. Bioelectron. 71, 1-6.

Tian, L., Bayen, S., Yaylayan, V., 2017. J. Anal. Appl. Pyrolysis 127, 120-125.

Vedova, P.D., Ilieva, M., Zhurbenko, V., Mateiu, R., Faralli, A., Dufva, M., Hansen, O., 2015. Small 11(2), 248-256.

Wang, H.S., Liu, H.L., Wang, K., Ding, Y., Xu, J.J., Xia, X.H., Chen, H.Y., 2017. Anal. Chem. 89(21), 11366-11371.

Wang, M., Hu, M., Liu, J., Guo, C., Peng, D., Jia, Q., He, L., Zhang, Z., Du, M., 2019. Biosens. Bioelectron. 132, 8-16.

Wang, S., Liu, J., Yong, W., Chen, Q., Zhang, L., Dong, Y., Su, H., Tan, T., 2015. Talanta 131, 562-569.

Wang, Y., Yang, M., Ren, Y., Fan, J., 2018. Anal. Chim. Acta 1040, 136-142.

Wienken, C.J., Baaske, P., Rothbauer, U., Braun, D., Duhr, S., 2010. Nat. Commun. 2010, 1, 100.

Wu, Y., Han, J., Xue, P., Xu, R., Kang, Y., 2015. Nanoscale 7(5), 1753-1759.

Xia, W., Mahmood, A., Zou, R., Xu, Q., 2015. Energy Environ. Sci. 8(7), 1837-1866.

Xu, H., Mi, H.Y., Guan, M.M., Shan, H.Y., Fei, Q., Huan, Y.F., Zhang, Z.Q., Feng, G.D., 2017. Food Chem. 232, 198-202.

Yan, C., Zhang, J., Yao, L., Xue, F., Lu, J., Li, B., Chen, W., 2018. Food Chem. 260, 208-212.

Yang, K., Hu, Y., Dong, N., 2016. Biosens. Bioelectron. 80, 373-377.

Yang, Q., Xu, Q., Jiang, H.L., 2017. Chem. Soc. Rev. 46(15), 4774-4808.

Yugender Goud, K., Hayat, A., Satyanarayana, M., Sunil Kumar, V., Catanante, G., Vengatajalabathy Gobi, K., Marty, J.L., 2017. Microchim. Acta 184(11), 4401-4408.

Zeissig, S., Blumberg, R.S., 2014. Nat. Immunol. 15(4), 307-310.

Zeng, J., Gan, N., Zhang, K., He, L., Lin, J., Hu, F., Cao, Y., 2019. Talanta 199, 491-498.

Zhang, G.Y., Zhuang, Y.H., Shan, D., Su, G.F., Cosnier, S., Zhang, X.J., 2016. Anal. Chem. 88(22), 11207-11212.

Zhang, H.T., Zhang, J.W., Huang, G., Du, Z.Y., Jiang, H.L., 2014a. Chem. Commun. 50(81), 12069-12072.

Zhang, K., Gan, N., Shen, Z., Cao, J., Hu, F., Li, T., 2019. Biosens. Bioelectron. 130, 139-146.

Zhang, K., Meng, X., Cao, Y., Yang, Z., Dong, H., Zhang, Y., Lu, H., Shi, Z., Zhang, X., 2018. Adv. Funct. Mater. 28(42).

Zhang, Q., Yu, J., Cai, J., Song, R., Cui, Y., Yang, Y., Chen, B., Qian, G., 2014b. Chem. Commun. 50(92), 14455-14458.

Zhao, M., Wang, Y., Ma, Q., Huang, Y., Zhang, X., Ping, J., Zhang, Z., Lu, Q., Yu, Y., Xu, H., Zhao, Y., Zhang, H., 2015. Adv. Mater. 27(45), 7372-7378.

Zheng, Y., Dou, X., Li, H., Lin, J.M., 2016. Nanoscale 8(9), 4933-4937.

Zhu, X., Li, B., Yang, J., Li, Y., Zhao, W., Shi, J., Gu, J., 2015. ACS Appl. Mater. Interfaces 7(1), 223-231.

Zhu, X., Zheng, H., Wei, X., Lin, Z., Guo, L., Qiu, B., Chen, G., 2013. Chem. Commun. 49(13), 1276-1278.

TOC figure

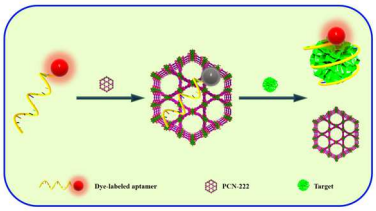

Highlights

- The strategy of fluorescence aptasensor for antibiotic detection was developed based on the very stable zirconium-porphyrin PCN-222 as a fluorescence quencher.
- The theoretical and experimental studied showed that the quenching mechanism of PCN-222 towards FAM-aptamer was both fluorescence resonance energy transfer (FRET) and photoinduced electron transfer (PET) processes with a high quenching efficiency.
- The proposed biosensor fulfilled the rapid, ultrasensitive and selective detection of chloramphenicol.
- The assay showed the potential and practical application for antibiotic detection in real food samples.

Credit author statement

The authors declare that they have no known competing financial interests or personal relationships that could have appeared to influence the work reported in this paper. All authors have contributed to editing and revising the paper. All authors have given approval to final version of manuscript.

Sha Liu: Methodology, Investigation, Validation and Writing-Original Draft.
Jialei Bai: Data curation, Formal analysis, Conceptualization and Writing-Original Draft.
Yapeng Huo: Software, Investigation, Validation and Writing-Original Draft.
Baoan Ning: Conceptualization, Writing-Original Draft and Supervision.
Yuan Peng: Conceptualization, Writing-Original Draft and Supervision.
Shuang Li: Resources and Writing-Original Draft.
Dianpeng Han: Project administration and Writing-Original Draft.
Weijun Kang: Conceptualization, Writing-Original/Reviewing and Editing, Supervision.
Zhixian Gao: Methodology, Funding acquisition, Writing-Original/Reviewing and Editing, Supervision.

Declaration of interests

☒ The authors declare that they have no known competing financial interests or personal relationships that could have appeared to influence the work reported in this paper.

☐The authors declare the following financial interests/personal relationships which may be considered as potential competing interests: